

# Binding Characteristics and Molecular Mechanism of Interaction between Ionic Liquid and DNA

Yuanhua Ding,<sup>†,‡</sup> Lin Zhang,<sup>‡</sup> Ju Xie,<sup>‡</sup> and Rong Guo<sup>\*,†,‡</sup>

School of Chemistry and Chemical Engineering, Nanjing University, Nanjing 210093, P. R. China, and School of Chemistry and Chemical Engineering, Yangzhou University, Yangzhou 225002, P. R. China

Received: November 2, 2009; Revised Manuscript Received: December 21, 2009

The binding characteristics and molecular mechanism of the interaction between a typical ionic liquid (IL), 1-butyl-3-methylimidazolium chloride ([bmim]Cl), as a green solvent and DNA were investigated for the first time by conductivity measurements, fluorescence spectroscopy, dynamic light scattering (DLS), cryogenic transmission electron microscopy (cryo-TEM), circular dichroism spectroscopy, <sup>31</sup>P nuclear magnetic resonance (NMR) spectroscopy, Fourier transform infrared spectroscopy, isothermal titration calorimetry (ITC), and quantum chemical calculations. It was found that the critical aggregation concentration of [bmim]Cl is decreased in the presence of DNA, and the addition of [bmim]Cl induced a continuous fluorescence quenching of the intercalated probe ethidium bromide (EtBr), indicating that the interaction between the ionic liquid and DNA is sufficiently strong to exclude EtBr from DNA. DLS results show that [bmim]Cl can induce a coil-to-globule transition of DNA at a low IL concentration, which was confirmed by the cryo-TEM images of DNA–IL complexes. With [bmim]Cl added, the resulting globular DNA structures and the extended DNA coils are first compacted, and then grow in size. During the binding process, DNA maintains the B-form, but the base packing and helical structure of DNA are altered to a certain extent. The <sup>31</sup>P NMR and IR spectra indicate that the cationic headgroups of bmim<sup>+</sup> groups interact with the phosphate groups of DNA through electrostatic attraction, and the hydrocarbon chains of bmim<sup>+</sup> groups interact with the bases through strong hydrophobic association. ITC results reveal the interaction enthalpy between [bmim]Cl and DNA and show that the hydrophobic interaction between the hydrocarbon chains of [bmim]Cl and the bases of DNA provides the dominant driving force in the binding. On the basis of quantum chemical calculations, it can be inferred that at a low IL concentration, the cationic headgroups of [bmim]Cl would be localized within several angstroms of the DNA phosphates, whereas the hydrophobic chains would be arranged parallel to the DNA surface. When the IL concentration is above 0.06 mol/L, the cationic headgroups are near DNA phosphates, and the hydrocarbon chains are perpendicularly attached to the DNA surface.

## Introduction

In recent years, ionic liquids (ILs) have attracted a great deal of attention due to their excellent chemical and physical properties, such as negligible vapor pressure, nonflammability, high chemical and thermal stability, low toxicity, good conductivity, and controllable hydrophobicity.<sup>1,2</sup> They have been widely considered as green solvents because of their potential as recyclable alternatives to the traditional organic solvents.<sup>2,3</sup> These unique properties of ILs offer great potential for applications in organic synthesis,<sup>4–7</sup> electrochemistry,<sup>8,9</sup> separation science,<sup>10–13</sup> material preparation,<sup>14–18</sup> and so on. At the present time, a burst of research activity in the field has been centered on the application of ILs in the life science. Ethylimidazolium tetrafluoroborate (EtImBF<sub>4</sub>) was used to successfully design an IL-containing ion conductive DNA film, which opened a new field of the use of DNA as a biomass.<sup>19,20</sup> A relatively stable capillary was prepared for DNA separation by coating an imidazolium-based IL.<sup>21</sup> Very recently, ILs were used to quantitatively extract trace amounts of DNA or cytochrome *c*.<sup>22,23</sup> In addition, ILs have also found application as ideal solvents or additives in immobilization and separation of

enzymes,<sup>24,25</sup> dissolution and regeneration of proteins,<sup>26</sup> and electrochemistry of biomacromolecules,<sup>9,27–29</sup> etc. However, all these applications, including the relevant properties, are related to the interaction between ILs and biomacromolecules.<sup>30</sup> It is therefore important to investigate the interaction between ILs and biomacromolecules for the understanding and development of applications of ionic liquids in life science.

DNA is one of the important biomacromolecules and is widely used in various life science investigations. However, there has been relatively little attention paid to the interaction between ILs and DNA since Erbeldinger et al. first used an anhydrous IL as an enzymatic catalysis medium to improve the stability and activity of enzymes.<sup>31</sup> Perhaps because ILs are almost completely inert species that do not produce optical, electric, and thermal signals, it is difficult to obtain the chemical and physical information on the interaction between ILs and biomacromolecules directly.<sup>30</sup> To date, only relatively little data is available on the interaction between ILs and DNA or protein. Qin et al. reported the electrostatic attraction between DNA fragments and one kind of dialkylimidazolium-based ILs, which was used to design an IL-coated capillary for DNA separation.<sup>21</sup> The interactions between cationic 1-butyl-3-methylimidazolium (bmim<sup>+</sup>) and P–O bonds of phosphate groups in the DNA strands were verified with <sup>31</sup>P NMR and Fourier transform infrared spectroscopy (FT-IR) spectra by Wang's group by using

\* To whom correspondence should be addressed. Phone: +86-514-87971802. Fax: +86-514-87975244. E-mail: guorong@yzu.edu.cn.

<sup>†</sup> Nanjing University.

<sup>‡</sup> Yangzhou University.

the ionic liquid 1-butyl-3-methylimidazolium hexafluorophosphate ( $[bmim]PF_6$ ) to extract dsDNA from an aqueous phase.<sup>22</sup> Recently, the surface electrochemical micromethod was applied to investigate the interaction between an ionic liquid 1-butyl-3-methylimidazolium tetrafluoroborate ( $[bmim]BF_4$ ) and DNA, in which the electrostatic interaction between  $[bmim]BF_4$  and DNA was suggested, and the thermodynamic and kinetic parameters, such as the binding constant, and the Gibbs energy of surface binding ( $\Delta G_b$ ) on a gold electrode, were obtained for the first time.<sup>30</sup>

However, the effects of ILs, as green solvents, on the structure and function of DNA, especially the molecular mechanism of the DNA–IL interaction, are still unclear. Furthermore, the thermodynamics governing the DNA–IL interaction is also important because it provides information on the structural properties of the IL complex with DNA. On the other hand, the above studies indicate that there exists an electrostatic interaction between ILs and DNA, which was revealed by  $^{31}P$  NMR and the surface electrochemical micromethod.<sup>22,30</sup> However, most ILs—for example, ILs based on the 1-alkyl-3-methylimidazolium cation  $C_nmim^+$ —possess an inherent amphiphility, and it can be expected that interfacial and aggregation behavior analogous to that exhibited by normal cationic surfactants may be displayed by these ILs.<sup>32</sup> Although the electrostatic interaction is essential in the interaction between ILs and DNA, the hydrophobic interaction between the alkyl chains of ILs and the bases of dsDNA is likely another important factor for the interaction between them. Thus, the role of hydrophobicity of ILs in the binding between ILs and DNA remains to be investigated.

In the present work, the binding characteristics and molecular mechanism of the interaction between a typical IL, 1-butyl-3-methylimidazolium chloride ( $[bmim]Cl$ ), and DNA were systematically investigated for the first time by means of conductivity measurements, fluorescence spectroscopy, dynamic light scattering (DLS), cryogenic transmission electron microscopy (cryo-TEM), circular dichroism (CD) spectroscopy, isothermal titration calorimetry (ITC),  $^{31}P$  nuclear magnetic resonance (NMR) spectroscopy, Fourier transform infrared spectroscopy, and quantum chemical calculations. The binding behavior of ILs on DNA, the coil–globule transition and the conformation change of DNA induced by ILs, and the thermodynamic behavior of the interaction between ILs and DNA were obtained. More importantly, the molecular mechanism of DNA–IL interaction was revealed by investigating the interaction sites. The authors are aware of the relevance of the results for the understanding of the interaction between ILs and DNA and provide the important theoretical basis for the application of ILs in life science.

## Experimental Section

**Materials.** The ionic liquid 1-butyl-3-methylimidazolium chloride was synthesized according to a method previously described, and the purity was checked by  $^1H$  NMR and FT-IR spectroscopy.<sup>6,12</sup> Deoxyribonucleic acid sodium salt from calf thymus (calf thymus DNA, ca. 10 kbp, D1501); the fluorescence probe, ethidium bromide (EtBr); and the component of Tris–HCl buffer solution (5 mM, pH = 7.4), tris(hydroxymethyl) aminomethane (Tris), were purchased from Sigma. Calf thymus DNA was used as received, since the purity of DNA is sufficiently high as determined from optical measurements. The ratio of the absorbance of the DNA stock solution at 260 nm to that at 280 nm was found to be 1.9, which suggested the absence of proteins.<sup>33</sup> Other chemicals employed were of analytical grade

and were also used without further purification. Deionized water (Super Q Millipore system, conductivity lower than  $18 \mu\text{s}\cdot\text{cm}^{-1}$ ) was used throughout.

A stock solution of DNA was prepared by dissolving an appropriate amount of the solid DNA in Tris–HCl buffer solution and stored at 4 °C for more than 24 h with occasional gentle shaking to get homogeneity. DNA concentrations were determined by using an extinction coefficient of  $6600 \text{ M}^{-1}\cdot\text{cm}^{-1}$  at 260 nm and expressed in terms of base molarity.<sup>34</sup> All samples used were prepared with Tris–HCl (5 mM, pH = 7.4).

**Conductivity and Fluorescence Measurements.** The conductivities of the ionic liquid solutions were measured with a DDS-11A digital conductivity meter (Shanghai Tianda Precision Instrument Co. Ltd.) calibrated using aqueous KCl solutions. The fluorescence emission spectra of free and DNA-associated ethidium bromide (EtBr, probe) were recorded with a Shimadzu 2501 spectrophotometer by varying the IL concentration and keeping the EtBr concentration constant. In all cases, both the excitation and emission band slits were fixed at 5 nm, and the fluorescence spectra were corrected for the background intensities of the buffer solution.

**Dynamic Light Scattering.** The dynamic light scattering experiments were performed with an ALV (CGS-8F) laser light scattering spectrometer working in a pseudocross-correlation mode, which was equipped with an ALV-6010/160 multiple tau digital real time correlator. A He–Ne laser was used as the light source with a output power of 25 mW and a maximum wavelength of 632.8 nm ( $\lambda$ ). The normalized intensity correlation functions  $g^{(2)}(q, \tau)$  were measured at a scattering angle of 70° and at a fixed temperature of 25 °C. For the data evaluation, the normalized electric field correlation function  $g^{(1)}(q, \tau)$  can be derived from the measured  $g^{(2)}(q, \tau)$  by the Siegert relation,<sup>35</sup>

$$g^{(2)}(q, \tau) = A \left[ 1 + \beta \left| g^{(1)}(q, \tau) \right|^2 \right] \quad (1)$$

where  $A$  is the measured baseline,  $\beta$  is the spatial coherence factor,  $q$  is the scattering wavevector, and  $\tau$  is the relaxation time.

For solutions containing monodisperse particles,  $g^{(1)}(q, \tau)$  decays exponentially with a decay rate  $\Gamma = Dq^2$ , where  $D$  is the translational diffusion coefficient, which is related to the hydrodynamic radius,  $R_H$ , by the Stokes–Einstein relation  $D = k_B T / 6\pi\eta R_H$ , where  $k_B$  is the Boltzmann constant,  $T$  is the absolute temperature, and  $\eta$  is the solvent viscosity. For solutions containing polydisperse particles, the correlation function  $g^{(1)}(q, \tau)$  no longer has a single-exponential decay and can be written as the Laplace transform of a continuous line-width distribution  $G(\Gamma)$  of decay times.

$$g^{(1)}(q, \tau) = \int_0^\infty G(\Gamma) \exp(-\Gamma\tau) d\Gamma \quad (2)$$

For the data evaluation, that is, the determination of  $G(\Gamma)$ , the distribution function of the diffusion coefficients from a  $g^{(1)}(q, \tau)$  inversion of this transformation has to be performed. From the distribution of  $D$ , the distribution of  $R_H$  can be easily calculated with the Stokes–Einstein equation. The analysis of the decay time distribution has been carried by the inverse Laplace transformation by means of a fit routine CONTIN,<sup>36</sup> which employs the constrained regularization method. All samples were also determined at scattering angles of 90° and

105°. This is to control if the second population that we observe does not derive from the internal motions of DNA.

**Cryogenic Transmission Electron Microscopy.** Transmission electron microscopy experiments under liquid nitrogen temperatures were conducted on a JEOL 2010 transmission electron microscope operated at 100 kV and equipped with a Gatan 655 liquid nitrogen specimen holder. Aqueous phase contrast was obtained at a nominal underfocus of 3–15  $\mu\text{m}$ . Images were recorded on a Gatan 832 multiscan digital camera.

Cryo-TEM samples were prepared as follows: A small droplet of each sample solution was placed on a carbon-coated, lacey film-supported, microperforated TEM copper grid. The excess solution of each sample was blotted with a piece of filter paper. Careful blotting produced thin liquid films with a thickness of 100–400 nm, which freely spanned the micropores of the TEM grids. The sample grids were then quickly plunged into liquid ethane and kept there before imaging.

**Circular Dichroism.** Circular dichroism measurements were performed on a JASCO J-810 spectrophotometer. The spectra were acquired in a 1.0 cm path-length quartz cuvette at 25 °C. Three scans were averaged per spectrum to improve the signal-to-noise ratio, operating from 220 to 320 nm at a scanning speed of 10 nm/min and a bandwidth of 1 nm. Measurements were performed under a constant nitrogen flow, which was used to purge the ozone generated by the light source of the instrument. The spectra were smoothed by using the noise-reducing option in the operating software of the instrument.

**$^{31}\text{P}$  NMR and FT-IR Spectroscopy.** The  $^{31}\text{P}$  NMR spectra of DNA in the presence of different concentrations of [bmim]Cl in Tris–HCl were recorded at 25 °C on a Bruker Avance 600 spectrometer. The measurements were carried out with a DDO probe at a resonance frequency of 242.88 MHz. The phosphorus chemical shifts of DNA were externally referenced to 85% orthophosphoric acid.

The FT-IR spectra of DNA, [bmim]Cl, and DNA–IL complex in Tris–HCl were recorded on a Bruker IFS66/S IR spectrometer by coaddition of 124 interferograms collected at a 4  $\text{cm}^{-1}$  resolution. The IR samples were prepared by spreading and drying the sample solutions on  $\text{CaF}_2$  infrared windows in a steady flow of dry nitrogen for at least 6 h.

**Isothermal Titration Microcalorimetry.** Isothermal titration calorimetry was performed with a VP-ITC calorimeter (Micro-Cal Inc., Century City, CA) at 25 °C. It has a reference cell and a sample cell, each of approximately 1.439 mL, and both cells are insulated by an adiabatic shield. The titration was carried out by injecting an IL solution of 1.0 mol/L from a 250  $\mu\text{L}$  rotating syringe into the sample cell filled with  $1.0 \times 10^{-5}$  mol/L DNA solution. The syringe tip acts as a blade-type stirrer to ensure an optimum mixing efficiency at 307 rpm. Each injection lasted 10 s, and there was an interval of 240 s between successive injections. A control experiment was conducted by injecting the IL solution into the sample cell containing only buffer under the same conditions. The corrected interaction heat was determined by subtracting the blank heat from that for the IL–DNA titration.

**Quantum Chemical Calculations.** The theoretical calculations were carried out using the Gaussian03 program for windows.<sup>37</sup> The optimization of the [bmim]Cl molecular structure and the corresponding structural parameters were obtained using density functional theory method at the UB3LYP level.<sup>38–40</sup> The split valence type basis set 6-31G(d,p) was used in the method.

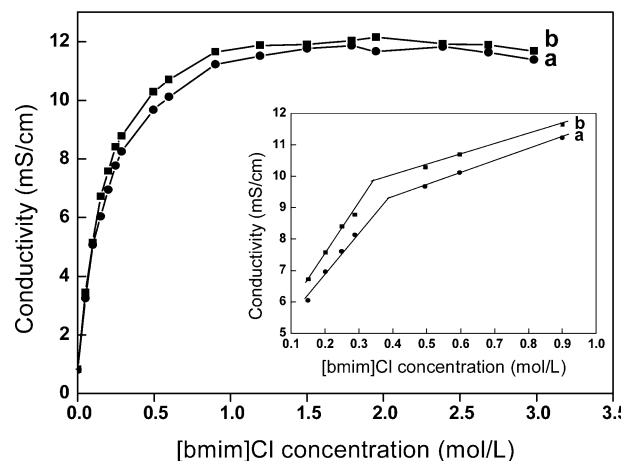


**Figure 1.** Electric conductivity ( $\kappa$ ) of [bmim]Cl solution as a function of [bmim]Cl concentration in the absence and presence of DNA. DNA concentration (mol/L): a, 0; b,  $1.0 \times 10^{-5}$ .

## Results and Discussion

**Conductivity Behavior.** The aggregation behavior of the ionic liquid [bmim]Cl in the presence of DNA was investigated by conductivity measurements. Figure 1 shows the variation of the electric conductivity of [bmim]Cl solution as a function of [bmim]Cl concentration in the absence and presence of DNA. As can be seen from curve a of Figure 1, the electric conductivity of [bmim]Cl solution in the absence of DNA first increases rapidly and then reaches a plateau with the IL concentration increasing. A distinct break on curve a, clearly shown by the inset of Figure 1, corresponds to a concentration of 0.39 mol/L, which can be defined as a critical aggregation concentration (cac).<sup>32</sup> Above the cac, the IL can form micelle-like aggregates due to its inherent amphiphilicity, which will be also revealed by the following studies. When the [bmim]Cl solution contained  $1.0 \times 10^{-5}$  mol/L DNA, as shown by curve b of Figure 1, a similar conductivity behavior is found. The conductivity values measured in the presence of DNA are a little greater than those obtained in the absence of DNA, which is ascribed to the contribution of  $\text{Na}^+$  ions and phosphate groups of DNA. However, the cac value is decreased to 0.34 mol/L in comparison with that in the absence of DNA, as shown by the inset of Figure 1. This indicates that an interaction between the ionic liquid and DNA occurs. Because the phosphate groups of DNA are negative, they can act as counterions to the cationic bmim<sup>+</sup> groups and, thus, practically neutralize the cationic groups through binding due to the electrostatic attraction. This will reduce the electric repulsion between the cationic groups of [bmim]Cl and facilitate their aggregation, resulting in a lower critical aggregation concentration.

**Fluorescence Quenching of DNA-Bound Ethidium Bromide Induced by Ionic Liquid.** Ethidium bromide (EtBr), as a fluorescence probe, binds DNA by intercalating into the base pairs of double-stranded DNA and stretches the double helix of DNA.<sup>41–44</sup> The fluorescence intensity of this probe increases remarkably upon the intercalation because the hydrophobic microenvironment found between the base pairs protects the probe from water molecules and molecular oxygen that may quench its fluorescence emission.<sup>45</sup> When DNA is condensed or compacted by an IL, EtBr intercalation is prevented, and as a result, the fluorescence intensity will be quenched because the probe will remain fully accessible to the bulk solvent. Thus, the change of the fluorescence intensity of the probe can be used to detect the change of DNA conformation. In Figure 2,

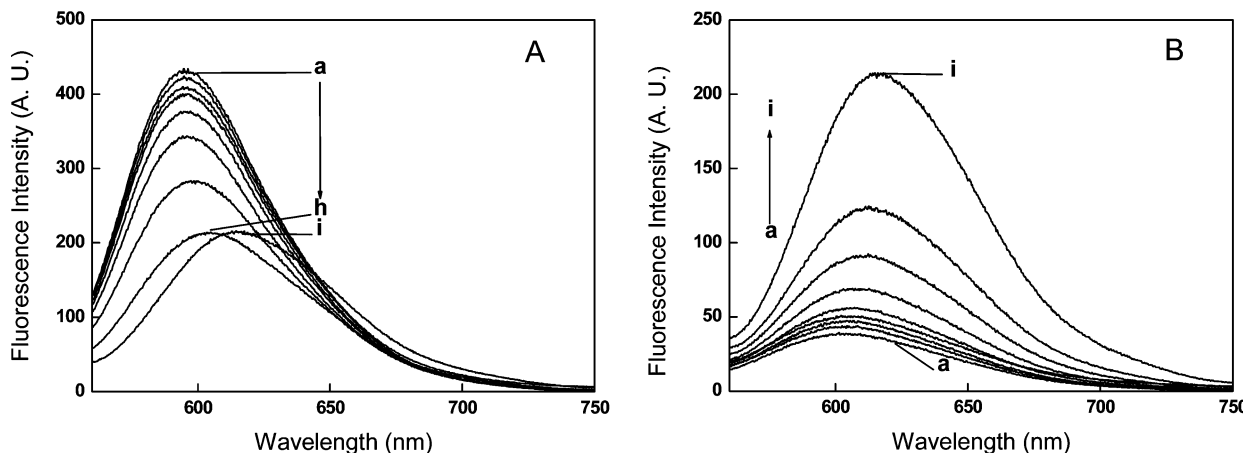


**Figure 2.** Fluorescence emission spectra of (A) DNA-bound ethidium bromide (probe) and (B) ethidium bromide in Tris–HCl solution ( $\text{pH} = 7.4$ ) containing different concentrations of  $[\text{bmim}] \text{Cl}$  at  $25^\circ\text{C}$ . DNA concentration:  $1.0 \times 10^{-5}$  mol/L. Ethidium bromide concentration:  $1.0 \times 10^{-5}$  mol/L.  $[\text{bmim}] \text{Cl}$  concentration (mol/L): a, 0; b, 0.04; c, 0.06; d, 0.08; e, 0.15; f, 0.25; g, 0.50; h, 1.0; i, 2.0.

the fluorescence emission spectra of free EtBr and DNA-bound species taken in Tris–HCl are displayed in the presence of  $[\text{bmim}] \text{Cl}$  with different concentrations. As shown in Figure 2A, DNA-bound EtBr exhibits a maximum emission peak around 595 nm when excited at 546 nm (curve a in Figure 2A). It can be seen from curves b–f that with increasing concentration of  $[\text{bmim}] \text{Cl}$  (0.04–0.25 mol/L), the fluorescence of DNA-bound EtBr is gradually quenched, and the emission peak position is almost unchanged. Upon further addition of  $[\text{bmim}] \text{Cl}$  (0.50–1.0 mol/L), the emission peak is gradually red-shifted from 595 to 602 nm in addition to the decrease in the fluorescence intensity (curves g–h in Figure 2A). When the  $[\text{bmim}] \text{Cl}$  concentration reaches 2.0 mol/L, the emission peak is remarkably red-shifted to 615 nm, with the fluorescence intensity almost unchanged (curve i in Figure 2A). If the  $[\text{bmim}] \text{Cl}$  concentration is further increased, the emission peak is gradually red-shifted, and the peak intensity is significantly increased (data not shown), which shows a spectral change similar to that shown by Figure 2B. The decrease in the fluorescence intensity in Figure 2A indicates that the interaction between the IL and DNA is sufficiently strong to displace the intercalation of EtBr in DNA.

The fluorescence quenching of DNA-bound EtBr upon the addition of  $[\text{bmim}] \text{Cl}$  may arise from the exclusion of EtBr from the DNA base pair microenvironment toward the aqueous bulk. As the cationic  $\text{bmim}^+$  groups bind to DNA by electrostatic attraction, a compact DNA structure is formed. The resulting DNA structure leaves insufficient space available for EtBr intercalation, leading to gradual release of EtBr from DNA and, thus, the decrease in the fluorescence intensity of EtBr. The dissociation of EtBr from the EtBr–DNA complex can be further revealed by the red shift of the emission peak. When the IL concentration is above its cac, as shown by curves g–i in Figure 2A, the emission peak is gradually red-shifted with the IL added. This implies that the released probe moves toward a different microenvironment; that is, the micelle-like aggregates of  $[\text{bmim}] \text{Cl}$  formed at the concentration above its cac. To confirm the above analysis, the fluorescence emission spectra of free EtBr in the presence of different concentrations of  $[\text{bmim}] \text{Cl}$  were measured under the same conditions (Figure 2B). As shown in Figure 2B, free EtBr exhibits a maximum emission around 602 nm at an excitation wavelength of 546 nm (curve a in Figure 2B). With  $[\text{bmim}] \text{Cl}$  added to the system from 0.04 to 2.0 mol/L, the fluorescence intensity is gradually increased, and the emission peak is gradually red-shifted from

602 to 615 nm (curves b–i in Figure 2B). Because the  $[\text{bmim}] \text{Cl}$  molecule shows amphiphility, it can form two- or three-molecule aggregates at the concentration below its cac and can form micelle-like aggregates at the concentration above its cac.<sup>32</sup> These aggregates contain a hydrophobic microdomain formed by the alkyl chains of  $[\text{bmim}] \text{Cl}$ , which will provide a hydrophobic microenvironment for EtBr solubilization. Furthermore, the hydrophobic microdomain of the formed aggregates becomes larger with the increasing IL concentration. This makes more and more EtBr molecules solubilized into the aggregates with the IL concentration increase, resulting in the increase in the local concentration of EtBr in the aggregates. Correspondingly, the effective absorption cross-sectional area increases, and the coupling of the conjugated EtBr molecules occurs. As a result, the fluorescence intensity of EtBr increases, and the emission peak is red-shifted with added  $[\text{bmim}] \text{Cl}$ , which is similar to the sensitization of photoactive molecules in micelles.<sup>46,47</sup> On the basis of the fluorescence features of free EtBr in the presence of  $[\text{bmim}] \text{Cl}$  (Figure 2B), it can be inferred from the red shift of the emission peak of DNA-bound EtBr that EtBr was released from EtBr–DNA complexes with added  $[\text{bmim}] \text{Cl}$ , and the released EtBr then moved toward the hydrophobic microdomain of the formed aggregates of  $[\text{bmim}] \text{Cl}$ . In addition, the increase in the fluorescence intensity of free EtBr with  $[\text{bmim}] \text{Cl}$  added in Figure 2B also indicates that the decrease in the fluorescence intensity of DNA-bound EtBr with  $[\text{bmim}] \text{Cl}$  added in Figure 2A was not ascribed to the direct quenching by the  $[\text{bmim}] \text{Cl}$  itself. It is noted that the resulting compacted DNA structure can retain the double-stranded organization, but the DNA conformation under this situation is changed, which will be verified by the following CD results.

The continuous decrease in the fluorescence intensity and the resulting red shift of emission peak of DNA-bound EtBr with added  $[\text{bmim}] \text{Cl}$  in Figure 2A also show that the fluorescence quenching was driven by the hydrophobic interactions between the hydrocarbon chains of  $[\text{bmim}] \text{Cl}$  and the bases of DNA, which form a hydrophobic interior of DNA<sup>45,48</sup> and between the hydrocarbon chains of  $[\text{bmim}] \text{Cl}$  binding on the surface of DNA. From the base pair amount of calf thymus DNA ( $\sim 10\ 000$  bp),<sup>49</sup> it can be estimated that the concentration of the phosphate groups is about 0.20 mol/L in  $1.0 \times 10^{-5}$  mol/L DNA solution. If the fluorescence quenching is induced only by the electrostatic binding, fluorescence will be unchanged after the negative phosphate groups of DNA are completely neutralized by cationic  $\text{bmim}^+$ , which corresponds to an IL concentration of 0.20 mol/L.

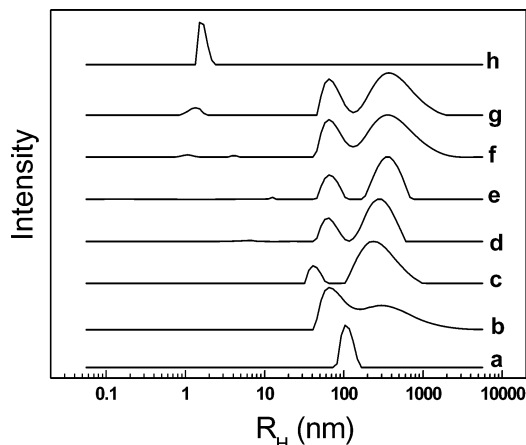


**Figure 3.** Intensity-weighted distribution functions of  $1.0 \times 10^{-5}$  mol/L DNA solution in the absence and presence of [bmim]Cl at 25 °C and a scattering angle of 70°. [bmim]Cl concentration (mol/L): a, 0 (only DNA); b, 0.02; c, 0.06; d, 0.08; e, 0.10; f, 0.50; g, 1.0. Curve h is 1.0 mol/L [bmim]Cl in Tris–HCl solution without DNA.

L. However, the fluorescence intensity continues to decrease with added [bmim]Cl, even though the IL concentration reaches 0.25 mol/L, as shown by curves f–h in Figure 2A. This indicates that although the electrostatic interaction is essential in the binding between [bmim]Cl and DNA, the hydrophobic interactions between the hydrocarbon chains of [bmim]Cl and the bases of DNA, and among the hydrocarbon chains of [bmim]Cl binding on the DNA, provide the main driving force. Such hydrophobic interactions cause a stronger condensation of DNA, which yields a very compact structure of an EtBr intercalated double helix structure, disrupting the controlling forces responsible for noncovalent binding.<sup>50</sup> The above results indicate that [bmim]Cl binds to DNA by the electrostatic attraction and strong hydrophobic association between the hydrocarbon chains of the IL and the hydrophobic bases of DNA, which is further driven by the hydrophobic interaction between the hydrocarbon chains of [bmim]Cl binding on the surface of DNA.

**Microstructural Transition of DNA Induced by Ionic Liquid.** DLS was used to investigate the microstructural changes of DNA with [bmim]Cl concentration. The DNA concentration in these experiments was relatively low,  $1.0 \times 10^{-5}$  mol/L in Tris–HCl, so as to avoid the interaction between the molecules. In Figure 3 are displayed the intensity-weighted distribution functions of  $1.0 \times 10^{-5}$  mol/L DNA solution in the presence of different concentrations of [bmim]Cl. As shown by curve a in Figure 3, the intensity-weighted size distribution of the DNA solution without [bmim]Cl presents only one peak, corresponding to the translational mode of the extended DNA molecules. The average hydrodynamic radius of the free DNA is about 103 nm, which is approximate to that measured by DLS in studying the DNA condensation induced by the surfactants cetyltrimethylammonium (CTAB) and dodecyldimethylamine oxide [DDAO].<sup>51</sup>

When the added [bmim]Cl concentration is 0.02 mol/L, there appear two size distribution peaks, which correspond to about 65 and 320 nm, respectively (curve b in Figure 3). The former peak with a smaller hydrodynamic radius of about 65 nm can be attributed to the compacted DNA structures, and the latter one can be attributed to the extended DNA coils, both of which arise from the binding of [bmim]Cl to DNA. Similar phenomena have been observed recently in the studies of the DNA compaction and decompaction by surfactants or  $\beta$ -cyclodextrin.<sup>52,53</sup>

When the [bmim]Cl concentration is increased to 0.06 mol/L, the sizes of the compacted DNA structures and the extended

DNA coils are decreased to 42 and 240 nm, respectively (curve c in Figure 3). This indicates that both the compacted and extended DNA structures are further compacted with added [bmim]Cl, which confirms the above fluorescence results. However, with further addition of [bmim]Cl from 0.08 to 0.10 mol/L, the sizes of the compacted DNA structures and the extended DNA coils are gradually increased to 65 and 360 nm, respectively (curves d–e in Figure 3), suggesting a continuous binding of [bmim]Cl to DNA. When the [bmim]Cl concentration reaches 0.50 mol/L, which is just above its cac, the above two size distribution peaks are almost unchanged, but another new peak appears around 1.4 nm with relatively low amplitude (curve f in Figure 3). Considering that the IL concentration is above its cac, the new peak around 1.4 nm can be attributed to small micelle-like aggregates of [bmim]Cl. Thereafter, this new peak increases in amplitude, whereas the other two size distribution peaks remain still unchanged (curve g in Figure 3).

To verify the formation of the micelle-like aggregates of [bmim]Cl at the concentration above 0.50 mol/L, a DLS experiment was performed on a 1.0 mol/L [bmim]Cl solution without DNA, which had the same IL concentration as the sample corresponding to curve g in Figure 3. As shown by curve h in Figure 3, a size distribution peak appears around 1.6 nm, which is very close to the new peak around 1.4 nm for the sample in the presence of DNA (curve g in Figure 3). Thus, the resulting new peak around 1.4 nm can be attributed to the formation of the micelle-like aggregates of [bmim]Cl (curves f–g in Figure 3), which is consistent with the red shift of the emission peak of DNA-bound EtBr with the [bmim]Cl concentration above 0.50 mol/L (curves g–i in Figure 2A). In addition, the size of the formed [bmim]Cl aggregates approaches that of the micelles formed by the IL, 1-butyl-3-methylimidazolium octyl sulfate ([C<sub>4</sub>mim][C<sub>8</sub>SO<sub>4</sub>]),<sup>54</sup> indicating that the obtained size of the micelle-like aggregates of [bmim]Cl is reasonable. These facts indicate that the binding of [bmim]Cl to DNA reaches saturation after the IL concentration reaches 0.50 mol/L, and the excess [bmim]Cl begins to form the micelle-like aggregates. From the above results, it can be seen that a significant change of the DNA structure occurs upon addition of [bmim]Cl.

The change in the DNA structures is ascribed to the electrostatic binding of [bmim]Cl to DNA and the strong hydrophobic association between the hydrocarbon chains of [bmim]Cl and hydrophobic bases of DNA. When [bmim]Cl was added to the DNA solution, it was bound to DNA by the electrostatic interaction and hydrophobic interaction between the hydrocarbon chains of the IL and the hydrophobic bases of DNA. Such cooperative interactions can favor the DNA compaction and make the DNA–IL complexes to undergo a structural rearrangement, resulting in a significant structural transition of DNA. The resulting compacted DNA structures take on mostly hollow globule forms, which will be observed by cryo-TEM below.

On the other hand, the freely extended DNA coils becomes large, probably due to the binding of the IL to DNA (curve b in Figure 3). With the addition of [bmim]Cl into the DNA solution, both the compacted and extended DNA structures were further condensed due to the electrostatic and hydrophobic interactions between the IL and DNA, which was driven by the hydrophobic interaction between the hydrocarbon chains of [bmim]Cl binding on the DNA surface (curve c in Figure 3). However, with further addition of [bmim]Cl, both the condensed DNA structures inhibit the electrostatic and hydrophobic interactions between the IL and DNA due to the steric hindrance.

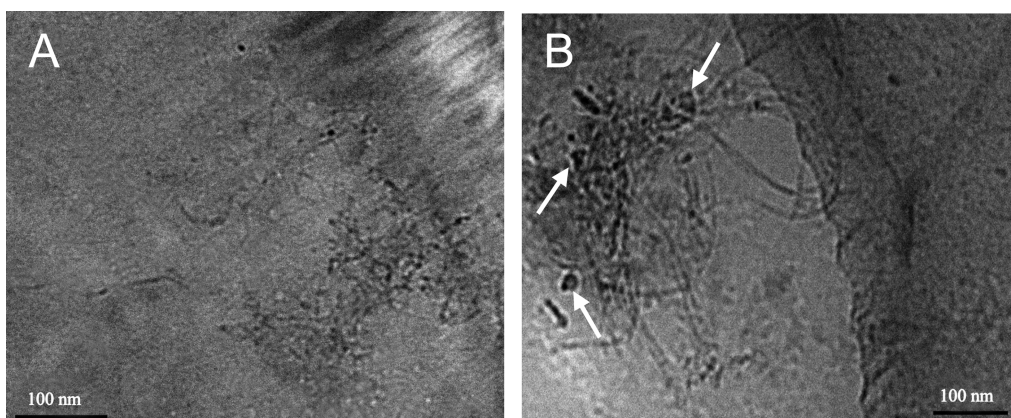


**Figure 4.** Cryo-TEM micrographs of (A) DNA in Tris–HCl solution and (B) DNA in the presence of 0.06 mol/L [bmim]Cl in the same buffer. The arrows indicate the globular particles of DNA induced by [bmim]Cl.

The added [bmim]Cl molecules interact only with those on the surface of DNA by the hydrophobic association of their hydrocarbon chains. In addition, the penetration of [bmim]Cl molecules into a DNA globule may also contribute to the increase in the size of the DNA globule. Therefore, the sizes of both the DNA structures increase with [bmim]Cl added after the IL concentration is above 0.06 mol/L (curves d–e in Figure 3).

Finally, the binding of [bmim]Cl on DNA reached saturation, and the micelle-like aggregates of [bmim]Cl were formed (curves f–g in Figure 3). It is noted that the peak, corresponding to a lower hydrodynamic radius, was not due to the internal modes of DNA, but due to the compacted DNA structures, which was checked by performing angular dependence experiments at 90° and 105°. In conclusion, [bmim]Cl, as a green solvent, can induce the structural changes of DNA by the electrostatic binding and hydrophobic association between the hydrocarbon chains of [bmim]Cl and the hydrophobic interior of DNA, resulting in a coil-to-globule transition, which is now reported for the first time.

In comparison with the cationic surfactants, such as CTAB, the binding strength of the IL on DNA is lower than that of the cationic surfactants on DNA due to the relatively weak electrostatic and hydrophobic interactions between the IL and DNA, which arise from the relatively large cationic  $\text{bmim}^+$  group and the relatively short hydrocarbon chain of the IL. As a result, a complete coil–globule transition induced by the IL does not occur, whereas the cationic surfactant CTAB can completely condense DNA into the compacted structures, that is, DNA globules, in the presence of higher concentration of CTAB.<sup>52,55,56</sup>

**Cryo-TEM Images of DNA–IL Complexes.** To confirm the microstructure of DNA–IL complexes, cryo-TEM was used to examine the morphology of the complexes. The typical cryo-TEM images of DNA in the absence and presence of [bmim]Cl are shown in Figure 4. As shown in Figure 4A, DNA itself shows an extended coiled structure with a large contour length. The diameter of DNA is about 4 nm, which is slightly larger than that of 2 nm obtained from X-ray diffraction.<sup>57</sup> The increase in the diameter of DNA is probably due to the hydration layer on the hydrophilic surface of DNA in Tris–HCl. When [bmim]Cl was added to the DNA solution, it can be seen from Figure 4B that the coiling extent of DNA is increased. Meanwhile, the globular particles of DNA appear with a size of 28–40 nm (shown as the arrows in Figure 4B), which corresponds to the size distribution peak with a smaller hydrodynamic radius in the presence of the same concentration

of [bmim]Cl (curve c in Figure 3). Furthermore, the white patches observed in these particles suggest that the resulting compacted DNA structures may be somewhat porous, which was confirmed by the unchanged contrast difference between the center and edge in the TEM images of one particle obtained when the sample grid was rotated by different degrees.

In addition, several rodlike DNA–IL complexes are also observed in Figure 4B. DLS results confirm the coil–globule transition of DNA induced by [bmim]Cl, and such an IL-induced transition has not been reported until now. It is noted that for the globular DNA, the hydrodynamic diameter obtained by DLS (about 84 nm, curve c in Figure 3) is larger than the size of 28–40 nm obtained by cryo-TEM under the same conditions. The apparently large difference comes from the different sizing method used by the manufacturers. Cryo-TEM gives the number-average diameter, whereas DLS gives a *z*-average diameter and also includes an aqueous hydration layer around the DNA globule. In addition, it can be also seen from Figure 4B that the diameter of DNA is increased from 4 to 11 nm with [bmim]Cl added. The large increase in the diameter of DNA suggests that cationic  $\text{bmim}^+$  groups are bound to the DNA surface and that the hydrocarbon chains of [bmim]Cl would not only be arranged parallel to the DNA surface, but also probably stand on the DNA surface. Therefore, the cryo-TEM results reveal the microstructure of DNA–IL complexes and confirms the coil-to-globule transition of DNA.

**Conformational Change of DNA Induced by Ionic Liquid.** To understand the change of the secondary structure of DNA during the binding process of [bmim]Cl to DNA, the circular dichroism spectrum of pure DNA and the spectra of DNA in the presence of different concentrations of [bmim]Cl are shown in Figure 5. The CD spectrum of the pure DNA shows a longwave, positive band at 278 nm corresponding to  $\pi-\pi$  base packing and a shortwave, negative band at 243 nm corresponding to helicity (curve a in Figure 5). The magnitude of the positive and negative bands are roughly equal with an intersection point at the absorption maximum. The above results are characteristic of the B-form of DNA.<sup>53</sup>

Upon addition of [bmim]Cl into the DNA solution, as shown by curves b–c in Figure 5, the CD spectra of [bmim]Cl-bound DNA show a shape similar to that of pure DNA in Tris–HCl, suggesting that DNA maintains the B-form in the presence of [bmim]Cl. However, the magnitudes of both the positive and negative bands increase with added [bmim]Cl; furthermore, the negative band is slightly shifted to a lower wavelength. This indicates that the addition of [bmim]Cl alters the base packing and helical structure of DNA to a certain extent, which is due

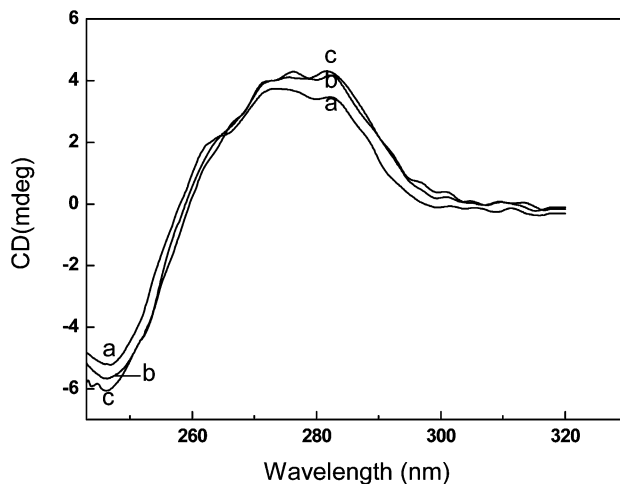


**Figure 5.** Circular dichroism spectra of  $5.0 \times 10^{-5}$  mol/L DNA at pH 7.4 in the presence of [bmim]Cl. [bmim]Cl concentration (mol/L): a, 0; b, 0.5; c, 1.0.

to the electrostatic interaction between the cationic  $\text{bmim}^+$  groups of [bmim]Cl and the phosphate groups of DNA and the hydrophobic interaction between the hydrocarbon chains of [bmim]Cl and the bases of DNA. In addition, the CD results support the previous fluorescence quenching of DNA-bound EtBr induced by [bmim]Cl (Figure 2A).

**Interaction Site Evidence of [Bmim]Cl on DNA from  $^{31}\text{P}$  NMR and IR Spectra.** The interaction site of [bmim]Cl on DNA was investigated by  $^{31}\text{P}$  NMR. The  $^{31}\text{P}$  NMR spectra of DNA in the presence of different concentrations of [bmim]Cl were measured, and the chemical shifts of DNA were externally referenced to 85% orthophosphoric acid (Figure S1 of the Supporting Information). The measured upfield  $^{31}\text{P}$  signals in the region of  $-12.0$  to  $-12.4$  ppm are assigned to the phosphate group with phosphor incorporated into a double-helix structure of DNA as a phosphodiester,<sup>58,59</sup> which arise from the lower electron negativity of the oxygen atoms attached to the phosphor atoms in DNA, as compared to those in phosphoric acid. The  $^{31}\text{P}$  signal from the phosphodiester of pure DNA appears at  $-12.2256$  ppm (curve a in Figure S1B), and it shifts gradually downfield to  $-12.2145$  ppm with added [bmim]Cl (curve e in Figure S1B).

A similar phenomenon had been observed in studying the intercalation of drugs, such as quinacrine and daunomycin, into DNA, in which these drugs produce a gradual downfield shift in the  $^{31}\text{P}$  signal of DNA.<sup>58</sup> The above results indicate that the cationic  $\text{bmim}^+$  groups interact with the phosphate groups of DNA by substituting the counterions attached to the P–O bonds, resulting in the corresponding change in the chemical environment for the P–O bonds. Meanwhile, the electronegativity of the oxygen atom is increased due to the electrostatic attraction of the cationic  $\text{bmim}^+$ ; thus, the  $^{31}\text{P}$  NMR signal of DNA is shifted downfield with added [bmim]Cl. However, the slight shift of the DNA  $^{31}\text{P}$  signal upon addition of the IL suggests that the electrostatic interaction between the  $\text{bmim}^+$  groups of [bmim]Cl and the phosphate groups of DNA, that is, the P–O–imidazolium bonding, is relatively weak in Tris–HCl.

To further characterize the interaction mechanism, IR spectroscopy was used to investigate the interaction site of [bmim]Cl on DNA. In Figure 6 are shown the FT-IR spectra for calf thymus DNA, [bmim]Cl, and DNA in the presence of 1.0 mol/L [bmim]Cl. As shown by curve a in Figure 6, the native DNA exhibits the characteristic absorption bands at  $1073$ ,  $1223$ , and  $1713\text{ cm}^{-1}$ , which are the marker absorption bands of the B-form

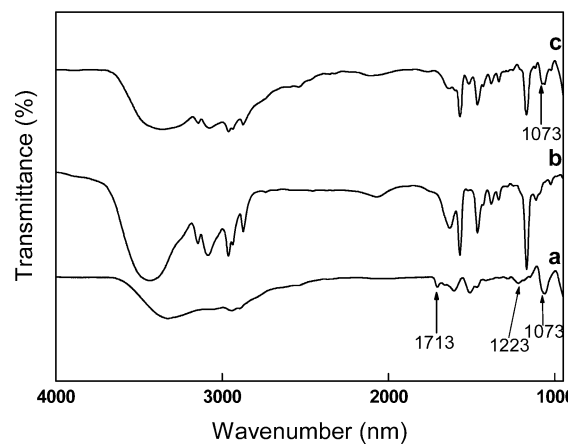


**Figure 6.** FT-IR spectra of (a)  $1.0 \times 10^{-5}$  mol/L DNA in Tris–HCl solution; (b) [bmim]Cl; and (c)  $1.0 \times 10^{-5}$  mol/L DNA solution in the presence of  $1.0$  mol/L [bmim]Cl.

of DNA, and consistent with the CD spectra. The IR bands at  $1073$  and  $1223\text{ cm}^{-1}$  are assigned to the symmetric and antisymmetric stretching vibrations of the  $\text{PO}_2^-$  groups of DNA, and that at  $1713\text{ cm}^{-1}$  is due to the in-plane  $\text{C}=\text{O}$  and  $\text{C}=\text{N}$  stretching vibrations of bases.<sup>60</sup> The above-mentioned absorption bands are not observed in the spectrum of [bmim]Cl (curve b in Figure 6). When [bmim]Cl was added into the DNA solution, the symmetric stretching vibration band of the  $\text{PO}_2^-$  groups at  $1073\text{ cm}^{-1}$  is almost unaffected, but the antisymmetric one at  $1223\text{ cm}^{-1}$  disappears (curve c in Figure 6). This indicates that the cationic  $\text{bmim}^+$  interacts with the phosphate groups of DNA through binding, which is due to the electrostatic attraction between them. However, the unchanged symmetric stretching vibration band at  $1073\text{ cm}^{-1}$  with the addition of [bmim]Cl implies that the electrostatic interaction between the cationic  $\text{bmim}^+$  and the phosphate groups of DNA is limited, and such interaction alters the helical structure of DNA only to a certain extent, which supports the CD and  $^{31}\text{P}$  NMR results. Furthermore, the disappearance of the IR band at  $1713\text{ cm}^{-1}$  in the presence of [bmim]Cl indicates that the base interactions are lost and the DNA double helix is partially denatured.

Such effects are still not found in studying the DNA compaction by cationic surfactants<sup>51–53</sup> or in studying the DNA extraction by the IL [bmim] $\text{PF}_6$ .<sup>22</sup> The disappearance of the IR band at  $1713\text{ cm}^{-1}$  also suggests that the hydrocarbon chains of [bmim]Cl interact with the bases of DNA through hydrophobic interaction. Therefore, although the electrostatic interaction between the cationic  $\text{bmim}^+$  and the phosphate groups of DNA is essential in the binding of [bmim]Cl on DNA, the hydrophobic interaction between the hydrocarbon chains of [bmim]Cl and the hydrophobic bases of DNA probably provides the dominant driving force.

**Thermodynamic Behavior of Interaction between Ionic Liquid and DNA.** Isothermal titration microcalorimetry (ITC) was employed to investigate the thermodynamic behavior associated with the interaction between [bmim]Cl and DNA. Figure 7 illustrates the ITC profile for the titration of  $1.0$  mol/L [bmim]Cl into the DNA solution and the corresponding differential enthalpy against the [bmim]Cl concentration, which was corrected by subtraction of the corresponding dilution heat derived from the injection of identical amounts of the IL into buffer alone. Such enthalpy measured in the ITC experiment is a sum of heat from several contributing sources, such as the dissociation of the micelle-like aggregates of [bmim]Cl into free unimers, the binding of [bmim]Cl on DNA due to the electro-

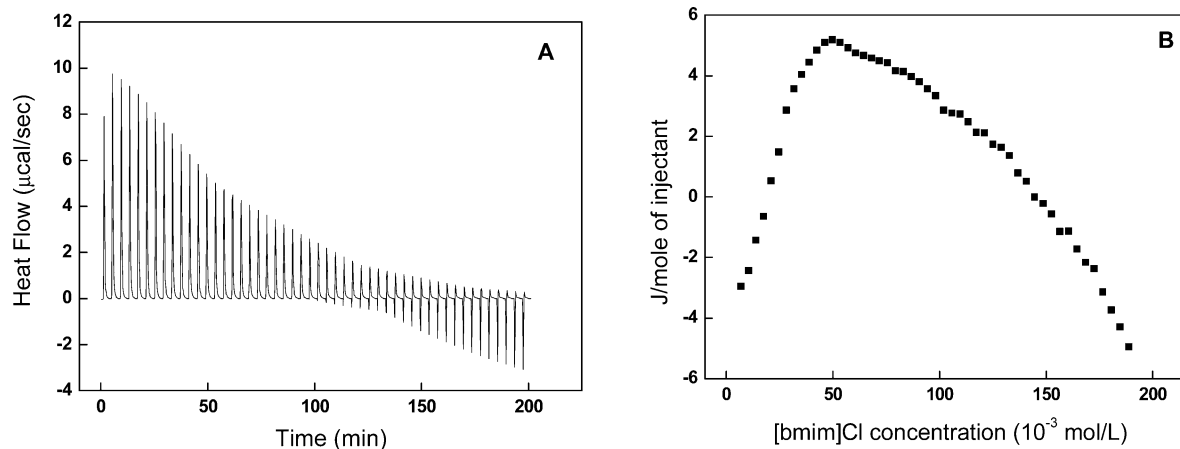


**Figure 7.** Calorimetric titration of  $[bmim]Cl$  into DNA solution at  $25.0\text{ }^{\circ}\text{C}$ . (Panel A) ITC profile of  $1.0 \times 10^{-5}\text{ mol/L}$  DNA titrated with  $1.0\text{ mol/L}$   $[bmim]Cl$  in Tris–HCl buffer solution. (Panel B) Corrected differential enthalpy against the  $[bmim]Cl$  concentration. The corrected differential enthalpies were derived by integration of the ITC profile shown in Figure 7A, followed by subtraction of the corresponding dilution heats derived from the control titrations of  $[bmim]Cl$  into buffer alone.

static and hydrophobic interactions, the dilution effect, and the change in the DNA conformation. Among these, the enthalpies from the dilution effect and the dissociation of  $[bmim]Cl$  aggregates were subtracted from a control titration of  $[bmim]Cl$  into the buffer alone.

From the first injection in Figure 7B, it can be seen that the observed enthalpy change is about  $-3.01\text{ J/mol}$ . Because the enthalpy of electrostatic interaction is close to zero or negligible,<sup>61,62</sup> the observed enthalpy change results mainly from the hydrophobic binding between the hydrocarbon chains of  $[bmim]Cl$  and the hydrophobic bases of DNA. This confirms that the hydrophobic interaction dominates over the electrostatic interaction and constitutes the driving force for the IL binding on DNA. Upon addition of  $[bmim]Cl$  into the DNA solution, the titration process changes from the exothermic enthalpy to a typical endothermic enthalpy, and the endothermic enthalpy reaches a maximum of  $5.23\text{ J/mol}$  at a  $[bmim]Cl$  concentration of  $0.05\text{ mol/L}$ . Generally, the binding of  $[bmim]Cl$  on DNA has a negative enthalpy, which is similar to the binding of the surfactant on protein.<sup>63</sup> Thus, the exothermic enthalpy in the first few injections may be contributed mainly from the hydrophobic binding between the hydrocarbon chains of the IL and the hydrophobic bases of DNA. Thereafter, the increasing endothermic enthalpy with addition of  $[bmim]Cl$  suggests that the structural rearrangement of the DNA–IL complexes probably occurs, which is consistent with the DLS and cryo-TEM results. Thus, the negative to positive enthalpy change may be due to the structural rearrangement of the DNA–IL complexes superimposed on the IL binding on DNA.

In addition, the dissociation of the hydration water molecules and counterions ( $\text{Na}^+$ ) from DNA also contributes to the endothermic response due to the competitive binding of  $\text{bmim}^+$  to DNA. When the IL concentration is larger than  $0.05\text{ mol/L}$ , the endothermic enthalpy changes gradually to the exothermic enthalpy with further addition of  $[bmim]Cl$  and eventually reaches  $-5.03\text{ J/mol}$ . This indicates that although the structural rearrangement of the DNA–IL complexes still occurs at this stage, the hydrophobic interaction between the added IL molecules and the DNA-bound IL molecules gradually becomes the main driving force for the IL binding on DNA. Correspondingly, the size of the DNA–IL complexes is increased with  $[bmim]Cl$  added, which is presented by the DLS results when the IL concentration is above  $0.06\text{ mol/L}$  (curves d–f in Figure 3). Furthermore, the IL concentration of  $0.05\text{ mol/L}$ , corre-

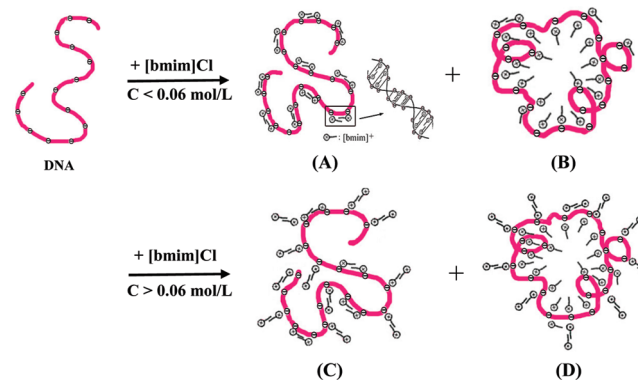


**Figure 8.** Schematic illustration of the interaction mechanism between the IL  $[bmim]Cl$  and DNA.

sponding to the maximum of the endothermic enthalpy in Figure 7, is close to that of  $0.06\text{ mol/L}$ , corresponding to the size transition of the DNA–IL complexes (curve c in Figure 3), which also supports the above analysis. Therefore, the binding behavior of  $[bmim]Cl$  on DNA, such as the binding amount, the DNA conformational change induced by the IL, and the binding mode, can be controlled by adjusting the molar ratio of the IL to DNA. However, it is difficult to obtain the binding constant and the binding stoichiometry of  $[bmim]Cl$  on DNA due to the multiple sets of interaction sites. In conclusion, the thermodynamic behavior of the interaction between  $[bmim]Cl$  and DNA clearly characterizes the binding feature of  $[bmim]Cl$  on DNA and confirms the  $^{31}\text{P}$  NMR and IR results.

**Binding Mode of Ionic Liquid on DNA.** On the basis of the above experimental evidence, a molecular mechanism of the interaction between the IL  $[bmim]Cl$  and DNA was proposed, as shown schematically in Figure 8. When the IL concentration is below  $0.06\text{ mol/L}$ , the individual  $[bmim]Cl$  molecules bind onto the DNA to form DNA–IL complexes. Specifically, the cationic  $\text{bmim}^+$  headgroups bind to the phosphate groups of DNA through electrostatic interaction, and the hydrocarbon chains of  $[bmim]Cl$  interact with the hydrophobic bases of DNA through hydrophobic interaction, as shown by the enlarged part of DNA in Figure 8A. Furthermore, the electrostatic and hydrophobic forces make the formed DNA–IL complexes undergo the structural transformation from coil to globule forms (Figure 8B), which means that the coil and globule forms coexist in the DNA solution. A similar coil-to-globule transition of DNA had been observed in studying

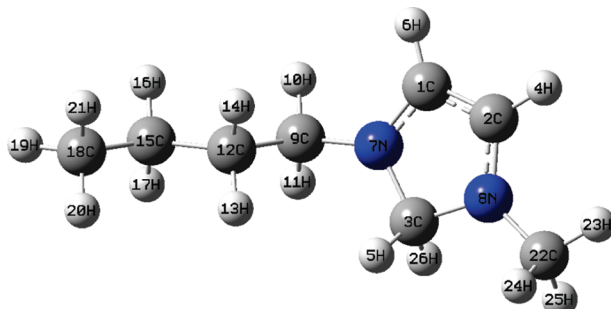


**Figure 9.** Optimized molecular structure of [bmim]Cl obtained from the DFT calculations.

DNA compaction by the cationic surfactant CTAB,<sup>52,55</sup> but the hydrophobic binding between the hydrocarbon chains of [bmim]Cl and the hydrophobic bases of DNA is not yet revealed by any technique until now. In addition, the hydrocarbon chains of the bound IL molecules could form the hydrophobic cores of the DNA globules due to the hydrophobic interaction between the hydrocarbon chains of the IL, as shown by the hollow DNA structures observed by cryo-TEM (Figure 4B). When the IL concentration is larger than 0.06 mol/L, both the coiled and globular DNA structures grow in their sizes with addition of the IL, which is due to the hydrophobic binding of the added IL molecules to the DNA-bound IL molecules on the DNA surface (Figure 8C–D). When the IL concentration reaches 0.50 mol/L, free micelle-like aggregates of [bmim]Cl begin to appear. During the binding process of [bmim]Cl to DNA, the hydrophobic interactions are the dominant driving force.

To confirm the molecular mechanism of the interaction between the IL and DNA, quantum chemical calculations were performed for the structural considerations. Figure 9 shows the optimized molecular structure of [bmim]Cl obtained from the DFT level of the theory, and the natural charges of the relevant atoms of the optimized molecule are listed in Table 1. The calculated results indicate that the positive unit charge of the cationic  $\text{bmim}^+$  group is a sum of all the atom charges. For the imidazole ring of  $\text{bmim}^+$  group, the net positive charge is only 0.378, obtained from the natural charges of the relevant atoms in Table 1, and the other positive charge of 0.622 is mostly distributed in the atoms of the hydrocarbon chain of the IL. It can be expected that the electrostatic interaction between the cationic  $\text{bmim}^+$  group and the phosphate group of DNA is nonspecific. Thus, it is relatively weak, which is consistent with the  $^{31}\text{P}$  NMR, IR, and ITC results. Considering that the positive charge of the conjugated imidazole ring is larger than that of the atoms of the hydrocarbon chain, the imidazole ring, i.e., the headgroup of [bmim]Cl, would be preferentially localized within several Å from DNA phosphates. It is known that the DNA diameter is equal to about 20 Å and phosphate charges are distributed every 1.7 Å along the DNA length.<sup>57</sup> Thus, the surface area of DNA per one negative charge is about 107 Å<sup>2</sup>. From the calculations, it can be also known that the  $\text{bmim}^+$  cation has a length of about 10.4647 Å and a width of about 4.0254 Å. Therefore, the hydrocarbon chain of a  $\text{bmim}^+$  cation can extend to the adjacent bases of DNA due to the hydrophobic interaction.

For full contact of the cationic  $\text{bmim}^+$  group with the phosphate group of DNA, the plane of the imidazole ring of

the IL would face to the DNA surface, and its hydrophobic tail would be arranged parallel to the DNA surface, displacing all or most water molecules from the DNA hydration layer. This will weaken the base interactions and cause the partial denaturation of the DNA double helix, which supports the CD, IR, and ITC results. Thus, it is reasonable that the hydrophobic interaction between the hydrocarbon chains of the IL and the bases of DNA is the dominant driving force for the structural transition during the binding process. The specific effect of the hydrocarbon chain length of ILs on the DNA structure is in progress in our lab. Furthermore, a bound  $\text{bmim}^+$  cation lying on its side may cover an area of about 40 Å<sup>2</sup>, which is only about 37% of the area needed to be filled with the cation. Therefore, the cationic  $\text{bmim}^+$  may lie down on the DNA surface and would have to cluster on the DNA surface.

The aggregation of the hydrocarbon chains of the bound IL molecules can minimize the exposure to the polarized microenvironment on the DNA surface. When the IL concentration reaches 0.06 mol/L, which is lower than that corresponding to a neutralizing amount of [bmim]Cl, the hydrophobic binding between the cationic  $\text{bmim}^+$  groups and the hydrophobic bases could be inhibited due to the relatively strong compaction and structural transition of DNA induced by the IL. As a result, the added cationic  $\text{bmim}^+$  is near DNA phosphates, whereas its hydrocarbon chain is perpendicularly attached to the DNA surface (Figure 8C–D). To remove the hydrocarbon chain from contact with water, some of the added IL molecules then bind to those bound on the DNA surface through the hydrophobic interaction, resulting in a remarkable increase in the sizes of the DNA structures (curves d–f in Figure 3). On the basis of the above analysis, the quantum chemical calculation results confirm the binding mechanism of the IL on DNA. The unique binding mode of the IL on the DNA surface results in the formation of functional DNA–IL complexes and the structure transition of DNA. The formed DNA–IL complexes with different structures suggest different potentials in the application of ILs to life science. For example, the compacted and extended DNA–IL complexes have different effects on the DNA extraction efficiency due to the different binding properties. Thus, it is feasible to improve the DNA extraction efficiency by changing the molar ratio of IL to DNA.

It is noted that the cationic surfactants, used to condense DNA, often induce surfactant-related cytotoxicity when they are used in life science, such as in cell transfection.<sup>64,65</sup> They are often used as model components for revealing the factor determining DNA interaction with cationic amphiphiles and for elucidation of the mechanism of this interaction.<sup>66</sup> Compared with the cationic surfactants, the ionic liquids are generally less harmful<sup>1,2,10,67</sup> and show excellent chemical and physical properties; thus, the formed DNA–IL complexes, in which the IL is used as a major or minor component, promise important application in life science, such as gene delivery, purification/separation of biomacromolecules, etc.

## Conclusions

The binding characteristics and molecular mechanism of the interaction between an ionic liquid [bmim]Cl as a green solvent and DNA were studied by means of various analytical techniques. The IL [bmim]Cl can bind to DNA effectively to form

**TABLE 1: Natural Charges of the Relevant Atoms of the Optimized [bmim]Cl Molecule Obtained from DFT Calculations**

numbered atom natural charge	C <sub>1</sub> 0.011	C <sub>2</sub> 0.013	C <sub>3</sub> −0.067	H <sub>4</sub> 0.281	H <sub>5</sub> 0.272	H <sub>6</sub> 0.281	N <sub>7</sub> −0.339	N <sub>8</sub> −0.346	H <sub>26</sub> 0.272
---------------------------------	-------------------------	-------------------------	--------------------------	-------------------------	-------------------------	-------------------------	--------------------------	--------------------------	--------------------------

DNA–IL complexes by the electrostatic attraction between the cationic  $\text{bmim}^+$  groups and DNA phosphates, and the hydrophobic association between the hydrocarbon chains of  $[\text{bmim}]Cl$  and the bases of DNA, which was driven by the hydrophobic interaction between the hydrocarbon chains of  $[\text{bmim}]Cl$  bound on the surface of DNA. Correspondingly, the enthalpy of the interaction between  $[\text{bmim}]Cl$  and DNA changes between  $-5.03$  and  $5.23 \text{ J/mol}$  with the IL added. At a low  $[\text{bmim}]Cl$  concentration,  $[\text{bmim}]Cl$  can induce the coil-to-globule transition of DNA; thus, the DNA structures can be adjusted by changing the IL concentration. During the binding process, DNA maintains the B-form, but its base packing and helical structure are altered to a certain extent. The headgroups of  $[\text{bmim}]Cl$  interact with the DNA phosphates, whereas the hydrocarbon chains of  $[\text{bmim}]Cl$  interact with the bases of DNA.

On the basis of the experimental evidence and the quantum chemical calculations, a molecular mechanism of the interaction between the IL and DNA was proposed. When the IL concentration is lower than  $0.06 \text{ mol/L}$ , the cationic headgroups would be localized within several angstroms from DNA phosphates, whereas the hydrophobic chains would be arranged parallel to the DNA surface. When the IL concentration is larger than  $0.06 \text{ mol/L}$ , the cationic headgroups of the added IL are near DNA phosphates, and the hydrocarbon chains are perpendicularly attached to the DNA surface. Although the electrostatic interaction is essential in the binding of  $[\text{bmim}]Cl$  to DNA, the hydrophobic interaction between the hydrocarbon chains of  $[\text{bmim}]Cl$  and the bases of DNA plays a dominant role. The unique binding mode of the IL on the DNA surface results in the formation of DNA–IL complexes with different structures. Due to the excellent properties of ILs, the formed DNA–IL complexes may promise important application in life science, such as gene delivery, purification/separation of biomacromolecules, etc.

**Acknowledgment.** This work was supported by the National Natural Science Foundation of China (20633010, 20773106).

**Supporting Information Available:**  $^{31}\text{P}$  NMR spectra of DNA in the presence of different concentrations of  $[\text{bmim}]Cl$  in Tris–HCl at  $25^\circ\text{C}$ . This material is available free of charge via the Internet at <http://pubs.acs.org>.

## References and Notes

- (1) Huddleston, J. G.; Visser, A. E.; Reichert, W. M.; Willauer, H. D.; Broker, G. A.; Rogers, R. D. *Green Chem.* **2001**, 156–164.
- (2) He, Y.; Li, Z.; Simone, P.; Lodge, T. P. *J. Am. Chem. Soc.* **2006**, 128, 2745–2750.
- (3) Seth, D.; Chakraborty, A.; Setua, P.; Sarkar, N. *Langmuir* **2006**, 22, 7768–7775.
- (4) Welton, T. *Chem. Rev.* **1999**, 99, 2071–2084.
- (5) Avery, T. D.; Jenkins, N. F.; Kimber, M. C.; Lupton, D. W.; Taylor, D. K. *Chem. Commun.* **2002**, 28–29.
- (6) Huddleston, J. G.; Rogers, R. D. *Chem. Commun.* **1998**, 1765–1766.
- (7) Smitana, M.; Mioskowski, C. *Org. Lett.* **2001**, 3, 1037–1039.
- (8) Fukumoto, K.; Yoshizawa, M.; Ohno, H. *J. Am. Chem. Soc.* **2005**, 127, 2398–2399.
- (9) Leone, A. M.; Weatherly, S. C.; Williams, M. E.; Thorp, H. H.; Murray, R. W. *J. Am. Chem. Soc.* **2001**, 123, 218–222.
- (10) Wasserscheid, P.; Keim, W. *Angew. Chem., Int. Ed.* **2000**, 39, 3772–3789.
- (11) Anderson, J. L.; Ding, J.; Welton, T.; Armstrong, D. W. *J. Am. Chem. Soc.* **2002**, 124, 14247–14254.
- (12) Chun, S.; Dzyuba, S. V.; Bartsch, R. A. *Anal. Chem.* **2001**, 73, 3737–3741.
- (13) Blanchard, L. A.; Brennecke, J. F. *Ind. Eng. Chem. Res.* **2001**, 40, 287–292.
- (14) Kim, K.; Demberelnyamba, D.; Lee, H. *Langmuir* **2004**, 20, 556–560.
- (15) Zhou, Y.; Antonietti, M. *J. Am. Chem. Soc.* **2003**, 125, 14960–14961.
- (16) Taubert, A. *Angew. Chem., Int. Ed.* **2004**, 43, 5380–5382.
- (17) Brezesinski, T.; Erpen, C.; Iimura, K.; Smarsly, B. *Chem. Mater.* **2005**, 17, 1683–1690.
- (18) Scheeren, C. W.; Machado, G.; Dupont, J.; Fichtner, P. F. P.; Texeira, S. R. *Inorg. Chem.* **2003**, 42, 4738–4742.
- (19) Nishimura, N.; Ohno, H. *J. Mater. Chem.* **2002**, 2299–2304.
- (20) Nishimura, N.; Nomura, Y.; Nakamura, N.; Ohno, H. *Biomaterials* **2005**, 26, 5558–5563.
- (21) Qin, W.; Li, S. F. Y. *Analyst* **2003**, 128, 37–41.
- (22) Wang, J. H.; Cheng, D. H.; Chen, X. W.; Du, Z.; Fang, Z. L. *Anal. Chem.* **2007**, 79, 620–625.
- (23) Shimojo, K.; Kamiya, N.; Tani, F.; Naganawa, H.; Naruta, Y.; Goto, M. *Anal. Chem.* **2006**, 78, 7735–7742.
- (24) Bagheri, M.; Rodríguez, H.; Swatloski, R. P.; Spear, S. K.; Daly, D. T.; Rogers, R. D. *Biomacromolecules* **2008**, 9, 381–387.
- (25) Shimojo, K.; Nakashima, K.; Kamiya, N.; Goto, M. *Biomacromolecules* **2006**, 7, 2–5.
- (26) Phillips, D. M.; Drummy, L. F.; Conrady, D. G.; Fox, D. M.; Naik, R. R.; Stone, M. O.; Trulove, P. C.; De Long, H. C.; Mantz, R. A. *J. Am. Chem. Soc.* **2004**, 126, 14350–14351.
- (27) Wang, S. F.; Chen, T.; Zhang, Z. L.; Shen, X. C.; Lu, Z. X.; Pang, D. W.; Wong, K. Y. *Langmuir* **2005**, 21, 9260–9266.
- (28) Lu, X.; Hu, J.; Yao, X.; Wang, Z.; Li, J. *Biomacromolecules* **2006**, 7, 975–980.
- (29) Wang, S. F.; Chen, T.; Zhang, Z. L.; Pang, D. W. *Electrochem. Commun.* **2007**, 9, 1337–1342.
- (30) Xie, Y. N.; Wang, S. F.; Zhang, Z. L.; Pang, D. W. *J. Phys. Chem. B* **2008**, 112, 9864–9868.
- (31) Erbeldinger, M.; Mesiano, A. J.; Russell, A. J. *Biotechnol. Prog.* **2000**, 16, 1129–1131.
- (32) Bowers, J.; Butts, C. P.; Martin, P. J.; Vergara-Gutierrez, M. C.; Heenan, R. K. *Langmuir* **2004**, 20, 2191–2198.
- (33) Saenger, W. *Principles of Nucleic Structure*; Springer-Verlag: New York, 1984.
- (34) Reichmann, M. E.; Rice, S. A.; Thomas, C. A.; Doty, P. *J. Am. Chem. Soc.* **1954**, 76, 3047–3053.
- (35) Chu, B. *Laser Light Scattering*, 2nd ed.; Academic Press: New York, 1991.
- (36) Provencher, S. W. *Comput. Phys. Commun.* **1982**, 27, 213–227.
- (37) Frisch, M. J.; Trucks, G. W.; Schlegel, H. B.; Scuseria, G. E.; Robb, M. A.; Cheeseman, J. R.; Zakrzewski, V. G.; Montgomery, J. A., Jr.; Stratmann, R. E.; Burant, J. C.; Dapprich, S.; Millam, J. M.; Daniels, A. D.; Kudin, K. N.; Strain, M. C.; Farkas, O.; Tomasi, J.; Barone, V.; Cossi, M.; Cammi, R.; Mennucci, B.; Pomelli, C.; Adamo, C.; Clifford, S.; Ochterski, J.; Petersson, G. A.; Ayala, P. Y.; Cui, Q.; Morokuma, K.; Malick, D. K.; Rabuck, A. D.; Raghavachari, K.; Foresman, J. B.; Cioslowski, J.; Ortiz, J. V.; Stefanov, B. B.; Liu, G.; Liashenko, A.; Piskorz, P.; Komaromi, I.; Gomperts, R.; Martin, R. L.; Fox, D. J.; Keith, T.; Al-Laham, M. A.; Peng, C. Y.; Nanayakkara, A.; Gonzalez, C.; Challacombe, M.; Gill, P. M. W.; Johnson, B. G.; Chen, W.; Wong, M. W.; Andres, J. L.; Head-Gordon, M.; Replogle, E. S.; Pople, J. A. *Gaussian 98, revision A.7*; Gaussian, Inc.: Pittsburgh, PA, 1998.
- (38) Becke, A. D. *Phys. Rev. A* **1988**, 38, 3098–3100.
- (39) Becke, A. D. *J. Chem. Phys.* **1993**, 98, 5648–5652.
- (40) Hay, P. J.; Wadt, W. R. *J. Chem. Phys.* **1985**, 82, 270–283.
- (41) Eastman, S. J.; Siegel, C.; Tousignant, J.; Smith, A. E.; Cheng, S. H.; Scheule, R. K. *Biochim. Biophys. Acta, Biomembr.* **1997**, 1325, 41–62.
- (42) Xu, Y. H.; Hui, S. W.; Frederik, P.; Szoka, F. C. *Biophys. J.* **1999**, 77, 341–353.
- (43) MacDonald, R. C.; Ashley, G. W.; Shida, M. M.; Rakhmanova, V. A.; Tarahovsky, Y. S.; Pantazatos, D. P.; Kennedy, M. T.; Pozharski, E. V.; Baker, K. A.; Jones, R. D.; Rosenzweig, H. S.; Choi, K. L.; Qiu, R.; McIntosh, T. J. *Biophys. J.* **1999**, 77, 2612–2629.
- (44) Tarahovsky, Y. S.; Koynova, R.; MacDonald, R. C. *Biophys. J.* **2004**, 87, 1054–1064.
- (45) Rodríguez-Pulido, A.; Ortega, F.; Llorca, O.; Aicart, E.; Junquera, E. *J. Phys. Chem. B* **2008**, 112, 12555–12565.
- (46) Bunton, C. A.; Sepulveda, L. *J. Phys. Chem.* **1979**, 83, 680–683.
- (47) Awan, M. A.; Shah, S. S. *Colloids Surf., A* **1997**, 122, 97–101.
- (48) Bhattacharya, S.; Mandal, S. S. *Biochim. Biophys. Acta, Biomembr.* **1997**, 1323, 29–44.
- (49) Zinchenko, A. A.; Sakaue, T.; Araki, S.; Yoshikawa, K.; Baigl, D. *J. Phys. Chem. B* **2007**, 111, 3019–3031.
- (50) Barreleiro, P. C. A.; Lindman, B. *J. Phys. Chem. B* **2003**, 107, 6208–6213.
- (51) Marchetti, S.; Onori, G.; Cametti, C. *J. Phys. Chem. B* **2005**, 109, 3676–3680.
- (52) Dias, R. S.; Innerlohinger, J.; Glatter, O.; Miguel, M. G.; Lindman, B. *J. Phys. Chem. B* **2005**, 109, 10458–10463.

- (53) Cao, M.; Deng, M.; Wang, X. L.; Wang, Y. *J. Phys. Chem. B* **2008**, *112*, 13648–13654.
- (54) Seth, D.; Sarkar, S.; Sarkar, N. *Langmuir* **2008**, *24*, 7085–7091.
- (55) Mel'nikov, S. M.; Sergeyev, V. G.; Yoshikawa, K. *J. Am. Chem. Soc.* **1995**, *117*, 2401–2408.
- (56) Mel'nikov, S. M.; Sergeyev, V. G.; Yoshikawa, K. *J. Am. Chem. Soc.* **1995**, *117*, 9951–9956.
- (57) Nelson, D. L.; Cox, M. M. *Lehninger Principles of Biochemistry*, 3rd ed.; Worth Publishers: New York, 2000.
- (58) Gorenstein, D. G.; Lai, K. *Biochemistry* **1989**, *28*, 2804–2812.
- (59) Overmars, F. J. J.; Pikkemaat, J. A.; van den Elst, H.; van Boom, J. H.; Altona, C. *J. Mol. Biol.* **1996**, *255*, 702–713.
- (60) Lee, S. L.; Debenedetti, P. G.; Errington, J. R.; Pethica, B. A.; Moore, D. J. *J. Phys. Chem. B* **2004**, *108*, 3098–3106.
- (61) Rungsardthong, U.; Ehtezazi, T.; Bailey, L.; Armes, S. P.; Garnett, M. C.; Stolnik, S. *Biomacromolecules* **2003**, *4*, 683–690.
- (62) Joshi, H.; Shirude, P. S.; Bansal, V.; Ganesh, K. N.; Sastry, M. *J. Phys. Chem. B* **2004**, *108*, 11535–11540.
- (63) Ding, Y. H.; Shu, Y.; Ge, L. L.; Guo, R. *Colloids Surf., A* **2007**, *298*, 163–169.
- (64) Pinnaduwage, P.; Schmitt, L.; Huang, L. *Biochim. Biophys. Acta* **1989**, *985*, 33–37.
- (65) Behr, J. P. *Acc. Chem. Res.* **1993**, *26*, 274–278.
- (66) Izumrudov, V. A.; Zhiryakova, M. V.; Gouliko, A. A. *Langmuir* **2002**, *18*, 10348–10356.
- (67) McCormick, R. M. *Anal. Biochem.* **1989**, *181*, 66–74.

JP9104757